

Dynamic light scattering investigations of nanoparticle aggregation following a light-induced pH jump

Ryan J. Murphy,^{a)} Denis Pristinski, Kalman Migler, Jack F. Douglas, and Vivek M. Prabhu^{b)}
*Polymers Division, National Institute of Standards and Technology, 100 Bureau Dr., Gaithersburg,
 Maryland 20899-8541, USA*

(Received 17 March 2010; accepted 15 April 2010; published online 19 May 2010)

There are many important processes where the stability of nanoparticles can change due to changes in solution environment. These processes are often difficult to study under controlled changes to the solution conditions. Dynamic light scattering was used to measure the initial kinetics of aggregation of carboxylated polystyrene nanoparticles after well-defined pH jumps using aqueous solutions of photoacid generator (PAG). With this approach, the pH of the solution was controlled by exposure to ultraviolet (UV) light without the delays from mixing or stirring. The aggregation kinetics of the nanoparticles was extremely sensitive to the solution pH. The UV exposure dose is inversely correlated with the resulting surface charge of the nanoparticles. Decreasing pH decreases the electrostatic repulsion force between particles and leads to aggregation. The reaction-limited or diffusion-limited aggregation kinetics was sensitive to the pH quench depth, relative to the acid-equilibrium constant (pK_a) of the surface carboxylic acid groups on the nanoparticles. Since numerous PAGs are commercially available, this approach provides a flexible method to study the aggregation of a variety of solvent-dispersed nanoparticle systems.

[doi:[10.1063/1.3425883](https://doi.org/10.1063/1.3425883)]

I. INTRODUCTION

The similarity of interactions and size of synthetic nanoparticles with natural protein “nanoparticles” makes them readily incorporated into biosystems. The uptake of synthetic nanoparticles by different cellular compartments with disparate pH and salt conditions will influence the particle-particle interactions. Identifying the effect of rapid changes in cellular environment on the stability of these nanoparticle dispersions is then necessary for the design of new materials, as well as classify nanoparticle hazards and toxicity. Specifically, the cytosolic pH is regulated to a value near 7.2, but within the lysosome, the pH is near 5.¹ Changes in such local solution conditions can then be expected to rapidly change the nanoparticle surface charge and surface chemistry by the competitive binding and exchange of adsorbed proteins and ligands. This may cause these particles to become unstable and aggregate or self-assemble, drastically changing their designed functions. Much work has been done to understand nanoparticle stability upon varying the solution pH conditions in relation to materials science applications. The behavior of Au,²⁻⁵ hematite,⁶ latex,^{5,7,3} silica,^{5,8,3,9} dendrimer,^{10,11} and proteins,¹² as well as Au/DNA hybrid materials^{13,14} points to the relevance of pH changes on the stability of particle dispersions in cellular environments.

The focus of the present work is to develop a method to measure the dynamics and kinetics of particle aggregation processes under nonequilibrium conditions. We introduce a

unique experimental approach to measure the early time aggregation by taking advantage of rapid and controlled pH jumps by using aqueous solutions of photoacid generators (PAGs). PAGs are important additives used in polymer thin film photoresist materials for photolithography.¹⁵ The PAGs are molecularly mixed in the thin polymer film, and upon exposure to UV light through a patterned mask, they undergo photolysis to form superacids. During a heating step, the acidic protons (photoacids) diffuse and catalyze a reaction on the acid-sensitive polymer to change the local polymer solubility for dissolution in an aqueous hydroxide solution. Many PAGs are available in ionic and nonionic forms; however, ionic triphenylsulfonium salts are quite common due to their blend compatibility with polymer films, metal-free composition, and high acid strength. Currently, high-volume lithography of features smaller than 45 nm use water as an immersion fluid between the photoresist and lens elements. While this reduces the wavelength and increases the resolution of patterning, early problems included the partial dissolution of PAGs into the water.^{16,17} This was exacerbated by enrichment of the PAG to the film surface and PAG water solubility, but could be controlled by the perfluoroalkylsulfonate molecular mass of the PAG.

The triflic acid based PAG is highly soluble in water^{18,19} and is a suitable candidate to induce pH jumps in nanoparticle solutions. The photolysis of the dissolved PAGs was induced by absorption of ultraviolet-visible (UV-vis) light with a well-defined exposure dose. The stability of the solution was continuously probed by dynamic light scattering (DLS) using a nonabsorbing wavelength of laser light before and after the pH jump. This has the advantage that no external flow fields (shear and rotation) are imposed that occurs

^{a)}Present address: CNRS-Rhodia-UPenn, Complex Assemblies of Soft Matter UMI 3254, Bristol, Pennsylvania 19007. Electronic mail: ryan.murphy@us.rhodia.com.

^{b)}Electronic mail: vprabhu@nist.gov.

during mixing and agitation so that the dynamics may be studied in a quiescent fluid state. Second, the approach does not incur any time delays, followed by external mixing and relaxation of flow fields, thus allowing us to probe over a wider time frame. The PAG solubility in water allows them to be used for *pH* dependent behavior of aqueous model nanoparticle systems, yet to our knowledge, there has been no reported study on the behavior of water-soluble PAGs in such complex fluids.

II. EXPERIMENTAL

A. Materials

The PAG, triphenylsulfonium triflate (TPS-triflate) (Sigma Aldrich, St. Louis, MO), was used as received. (Certain commercial equipment and materials are identified in this paper in order to specify adequately the experimental procedure. In no case does such identification imply recommendations by the National Institute of Standards and Technology nor does it imply that the material or equipment identified is necessarily the best available for this purpose.) The nanoparticle system used was carboxyl-stabilized polystyrene latex, 40 nm in diameter, with a stock concentration of 4% by mass to volume (Molecular Probes, Eugene, OR). Each solution was prepared by dilution of a nanoparticle stock solution to the desired concentration with a 1 g/L aqueous TPS-triflate solution and mixed with a vortex mixer for a minimum of 60 s.

B. *pH* jump

PAG and nanoparticle solutions were exposed by a UV light spot curing system, consisting of a high-pressure mercury vapor arc lamp, an optical filter with a UV-vis (320–500) nm transmission band filter, and a fiber optic guide with the 3 mm core diameter and the numerical aperture of 0.59. The light intensity at the light guide exit was 18 W/cm². The light guide exit was positioned above a low volume quartz spectroscopic cell, 2 cm above the solution. The light total divergence angle was 72°, corresponding to a circular illuminated spot in the air-solution interface plane with a diameter of 32 mm and a light intensity of 158 mW/cm². The horizontal cross section of the sample cell was 10 × 2 mm², corresponding to approximately 32 mW of light power utilized for acid generation. A calibration curve was developed to relate UV exposure dose to a directly measured *pH*. These *pH* measurements on PAG solutions without nanoparticles were done on ≈10 mL solutions, constantly stirred at room temperature. The exposure conditions ensured that the entire solution volume was exposed with similar UV light path length to the spectroscopic cell system. The uncertainty in the power is less than 3%, as determined by independent measurements. The solution was exposed in 1 s intervals for the first 10 s, then 10 s intervals thereafter. Each *pH* curve was generated from a single PAG solution, and the UV light blocked by a shutter after each exposure duration. Each PAG solution was tested at least three times to assure that each solution had a reproducible *pH* jump. The measured *pH* of the solution remained constant beyond the time scales of the DLS experiments. The photolysis process is

irreversible and *pH* drifts were not observed with samples protected from ambient light that could serve as a background exposure with these UV-sensitive solutions.

C. DLS

The aggregation behavior was monitored via custom DLS setup that utilizes a single-mode fiber-coupled diode-pumped solid state (DPSS) 532 nm laser. A collimated linearly polarized laser beam with a diameter of 0.9 mm was focused with a 180 mm focal distance achromatic doublet lens at the center of a low volume quartz cuvette. The focused light beam waist was 260 μm. The cell had internal dimensions of 10 × 2 mm² and required ≈0.1 mL of the solution. The quasielastically scattered light at 90°, passed through a linear polarizer, and was coupled by an 8 mm focal distance aspheric lens to a single-mode fiber with 4.3 μm core size and 0.12 numerical aperture.

The fiber was connected to two photomultiplier tube photon counting modules with 28% detection efficiency at the laser wavelength using a fused fiber 50:50 splitter. Photon counts were registered by a digital cross-correlation board with the 100 ns time resolution. The laser incident power of 8 mW was reduced by a set of neutral density filters to keep the photon count below 1 MHz per channel in the detectors' linear range. The spatial coherence value of 0.8 was limited by the DPSS laser mode hopping. All measurements were done at room temperature (24 °C).

The aggregate size was determined by analyzing the scattered light intensity time autocorrelation, $g_2(\tau)$, defined as $g_2(\tau) = \langle I(t)I(t+\tau) \rangle / \langle I(t) \rangle^2$, where $I(t)$ and $I(t+\tau)$ are the scattered intensities at some initial time t and some later time $t+\tau$, τ is the delay time, and averaging is done over the observation time t . The fluctuation correlation of light scattered from the particles will exponentially decay due to particles undergoing longer range motion at long times. For polydispersed systems, the spectrum of relaxation times of the particles can be calculated by fitting the time autocorrelation function with an exponential decay function integrated over the relaxation rate distribution $G(\Gamma)$,

$$g_2(\tau) = 1 + \beta' g_1^2(\tau), \quad g_1(\tau) = \int G(\Gamma) \exp(-\Gamma\tau) d\Gamma,$$

where $\Gamma = q^2 D$, $q = (4\pi n_o / \lambda) \sin(\Theta/2)$, D is the diffusion coefficient, n_o is the refractive index of the solvent, λ is the laser wavelength in vacuum, Θ is the scattering angle, and β' is an instrument alignment-dependent coherence factor. From this, the distribution of hydrodynamic radii (R_h) may be obtained through infinite dilution the Stokes–Einstein relationship, $D = k_B T / 6\pi\eta_o R_h$, where T is the solution temperature, k_B is Boltzmann's constant, and η_o is the solution viscosity where interparticle interaction effects are neglected, as appropriate at very low particle concentrations (0.001% by mass). This procedure yields a unimodal log-normal size distribution of particle aggregates was assumed for the data fitting.²⁰ This analysis and methodology has been previously applied for the DLS of latex dispersions.²¹ Here, we utilized a time-resolved *in situ* DLS technique as that sampled the solution dynamics in 5 s intervals as a function of *pH*.

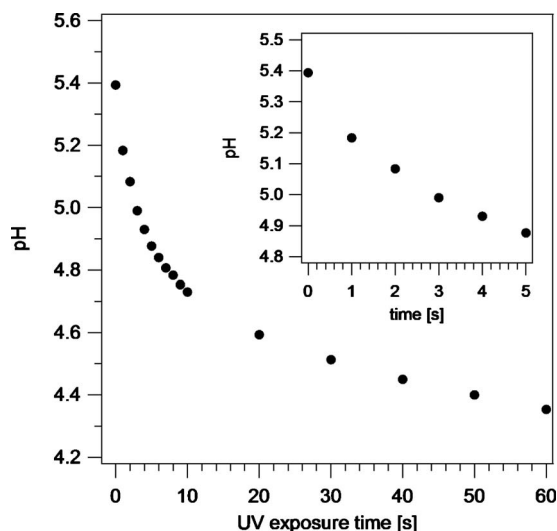


FIG. 1. Measured pH as a function of UV exposure time for 1g/l aqueous TPS-triflate solution. All the data are obtained from the same solution, and the UV light is turned off after each exposure time.

III. RESULTS AND DISCUSSIONS

A. pH quench methodology

One advantage of using PAG solutions to study nanoparticle stability over other mixing techniques is the lack of an induced flow field due to the acid generation being a product of a photolysis reaction. Also the PAG approach allows for a much wider range of accessible sample volumes to be tested. Theoretically, the rapid pH response of aqueous PAG solutions is limited by the solubility of the PAG and exposure conditions that impose the pH jump. Since ionic PAGs are essentially salts, they can effectively change the solution ionic strength; however, nonionic PAGs are also available. Therefore, a balance between solubility, PAG dispersion, and UV exposure must be considered. For this study, the optimal PAG system had to possess a high water solubility to allow for the most efficient proton generation per unit time of exposure, yet also allow the carboxyl-treated nanoparticles to be stable in solution. The triphenylsulfonium triflate PAG was selected based on its high water solubility (9 g/L).^{18,19} The solution pH versus UV exposure time is shown in Fig. 1 at a concentration of 1g/L, which is an experimentally determined maximum PAG concentration for stable nanoparticle suspensions without UV light exposure. UV exposure times less than 10 s were used for the DLS experiments in order to capture the initial aggregation kinetics with a large pH drop.

B. Nanoparticle suspension stability

The next step was to introduce carboxyl-stabilized latex nanoparticles (0.001% by mass) to the solution to test the stability as a function of UV induced acidification, with the DLS results shown in Fig. 2. The aggregation behavior was followed in real time with DLS; thus, as the particles started to aggregate, the corresponding relaxation time (τ) of the aggregates would systematically shift to longer times, which is clearly seen in the $g_2(\tau)$ contour plots shown in Fig. 2(a). For the pH 5.39 sample (no UV exposure), the nanoparticles do not aggregate, thus their $g_2(\tau)$ profiles do not change over

the course of the experiment. However, as the pH approaches 5.0, no change in the DLS spectrum appears within ≈ 100 s, after which the system appears unstable and aggregates with the relaxation time increasing. For $pH < 5.0$, the system is unstable and the nanoparticles immediately aggregate. The aggregation behavior for this system can be better seen when the correlation curves are fitted with a log-normal distribution, with the Stokes–Einstein relationship being used to calculate each R_h value from the measured relaxation time. Figure 2(b) displays the peak of the R_h distribution, $R_{h,peak}$, as a function of time after exposure. Our DLS measurements were performed at only single angle and we also assume the validity of the Stokes–Einstein relationship in our comparison between the hydrodynamic radii under different exposure conditions. A more complete approach would be to analyze the multiangle DLS to demonstrate diffusive scaling of the angular dependence of the relaxation rate. However, this type of measurement with common instrumentation would not allow us to follow the early time aggregation kinetics. We believe that the assumptions we make are a reasonable first approximation for our low concentrations of particles, but application of our method to higher concentrations will require an investigation of the angular dependence of the light scattering and hydrodynamic and excluded volume interaction effects that can affect D .

The lowering of the surface charge by the decreased pH reduces the stability of the nanoparticles. The stability of these nanoparticles is defined by the relative strength of the van der Waals attractive interactions of the polystyrene versus the electrostatic repulsion by the carboxylic acid groups on the particle surface. Because carboxylic acid has a pK_a of ≈ 4.7 , at neutral or basic solution pH values²² the nanoparticles are highly negatively charged and thus quite stable, hence why at $pH > 5.30$ there is no appreciable aggregation.

As the pH approaches the pK_a [inset in Fig. 2(b)], the kinetics exhibit an exponential growth rate, which is consistent with a reaction-rate limited cluster aggregation (RLCA) model. Lin *et al.*⁵ described this phenomenon extensively where this growth region is characterized by the reaction time for two particles to stick being longer than their collision time. Here, the reaction time is governed by the balance between the electrostatic repulsion and van der Waals forces. In this case, the pH of the solution becomes commensurate with the pK_a of the carboxylic acid group, resulting in a reduced average surface charge. This results in a slower rate of aggregation formation, followed by an increased rate at later times due to the probability of binding being proportional to the size of the slowly growing aggregates. The initial growth rate was shown to be exponential,⁵ and the data for pH 5.03 and 5.01 displayed a good fit to $R_{h,peak} = Ae^{t/\beta}$, where t is the aggregation time after UV exposure, A is a prefactor that relates to the pre-exposure particle hydrodynamic radius, and β is the characteristic aggregation time constant. As previously observed for polystyrene nanoparticles,⁵ we find two distinct characteristic time constants; for $t < 550$ s, $\beta_{pH5.03} \approx (209 \pm 9)$ s and $\beta_{pH5.01} \approx (275 \pm 10)$ s and for $t > 550$ s, $\beta_{pH5.03} \approx (690 \pm 100)$ s and $\beta_{pH5.01} \approx (680 \pm 120)$ s. Uncertainties are calculated as the estimated 1 standard deviation from the mean. The ratio

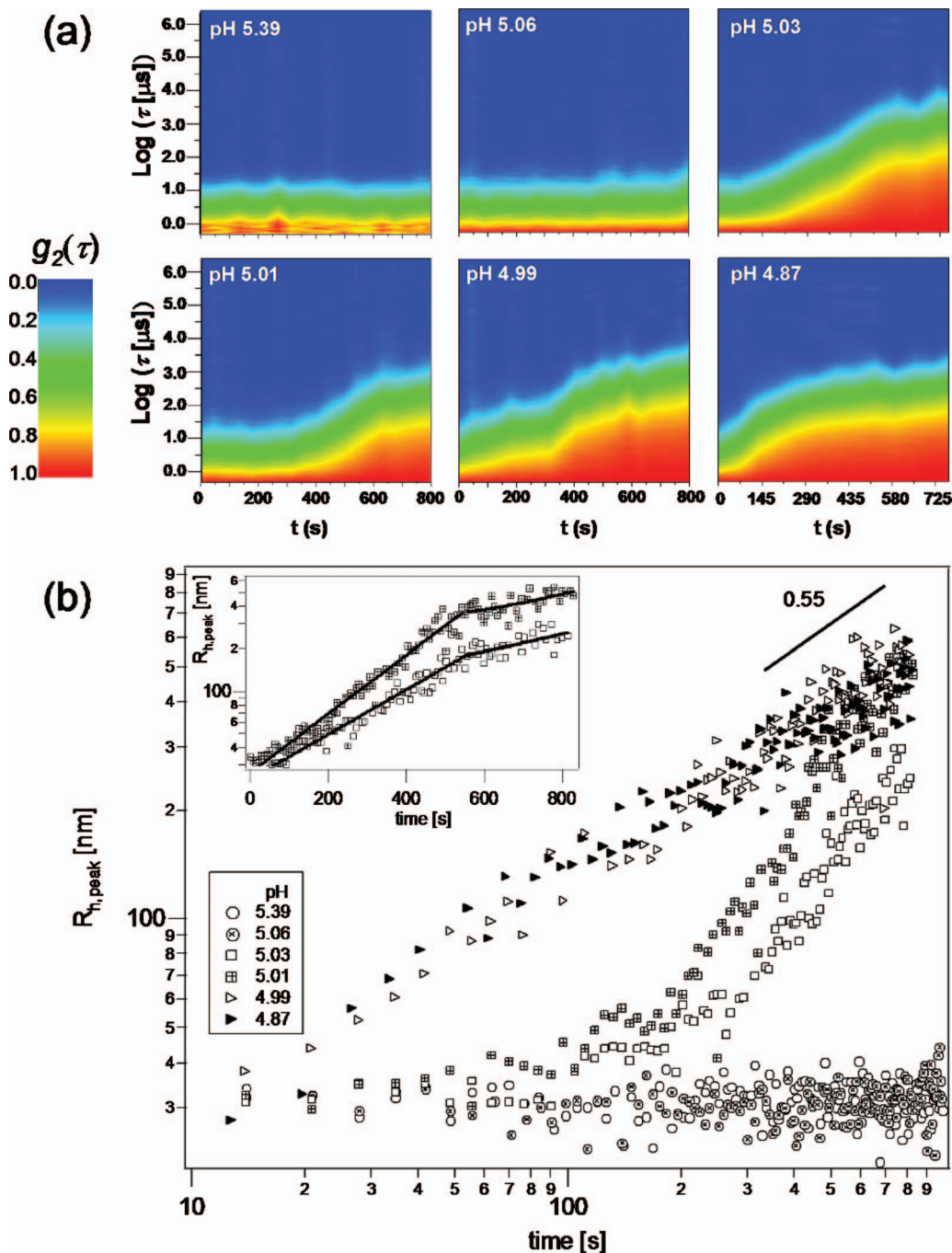


FIG. 2. (a) DLS normalized correlation function, $g_2(\tau)$, contour plots as a function of pH. For each plot, the abscissa is the *in situ* experimental time after UV exposure for the labeled plot and directly above and the ordinate is the logarithm of the correlation time τ equal scale for each graph. (b) $R_{h,\text{peak}}$ vs time after UV exposure as a function of pH. The inset is the pH 5.03 and 5.01 data plotted on a semilog scale with exponential fits as described in the main text.

of the characteristic times, $\beta_{r>550}/\beta_{r<550} \approx 3$, is similar to the results of Lin *et al.* for spherical polystyrene nanoparticles, whereby a cosolvent (2.6×10^{-6} mol/l pyridine) was added and agitated to destabilize the solution rather than pH.

As the pH is further decreased, the kinetics followed a power law form, consistent with diffusion-limited cluster aggregation (DLCA).³ This effect arises because of the reprotonation of the carboxylic acid dominates at $\text{pH} < \text{p}K_a$ and further reduces the surface charge, allowing for the attractive van der Waals forces to drive aggregation. In this case, the cluster size growth is limited by the rate of particle collisions, thus immediate and rapid aggregation is observed.

When fitted with a power law, $R_{h,\text{peak}} = At^\alpha$, the kinetic constant $\alpha \approx 0.55$ for $\text{pH} < 5.0$, equivalent to that found (≈ 0.52) by Lin *et al.* for gold nanoparticles within the uncertainty of the measurement. This kinetic constant $\alpha = z/d_f$, where d_f is the fractal dimension and z is theoretically expected to be 1, so the fractal dimension of the aggregate is 1.82. Recent results on metallic systems have similar qualitative behavior over a wider pH range, yet there was little discussion on the initial aggregation rate.⁶

The peak of the distribution (or mode value) quantifies the most probable aggregate size of the solution rather than the log-normal mean. The average of a log-normal distribu-

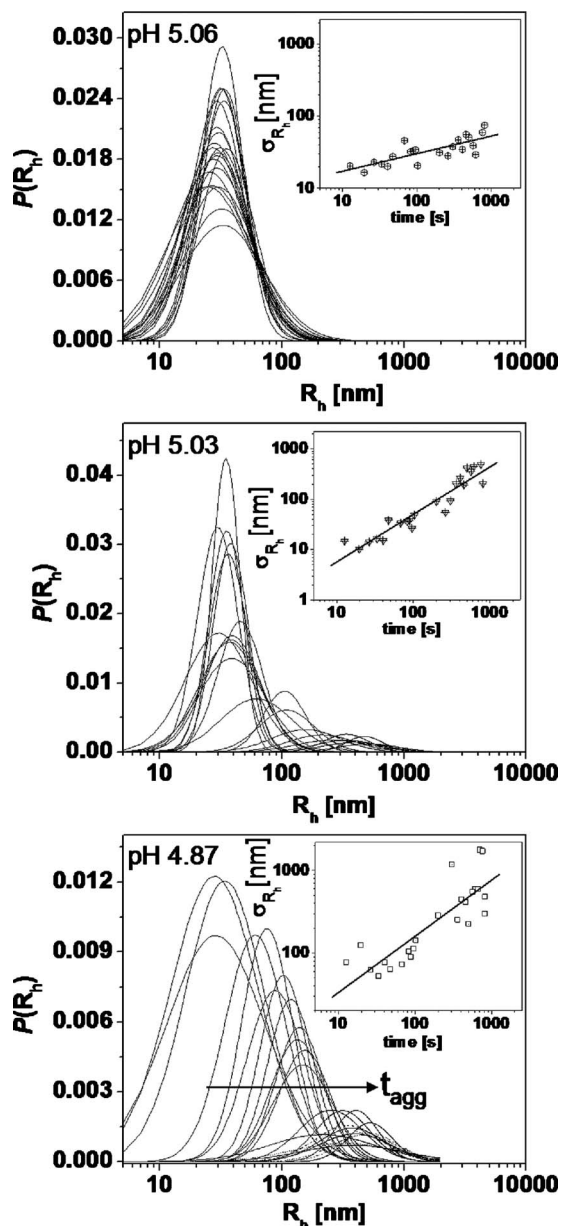


FIG. 3. Log-normal distributions for pH 5.06, 5.03, and 4.87 as a function of time after UV exposure. The insets are the standard deviation for each curve as a function of time. Lines are guides. As the pH quench is increased, the peak values ($R_{h,mode}$) shift to larger R_h . The standard deviation (σ_{R_h}) of R_h increases with time at a faster rate at lower pH. Overall, the aggregate size and distribution increase with time.

tion depends on the variance and skewness; thus, a separate analysis of the distributions peak and standard deviation (or square root of the variance) is appropriate. This is illustrated by the results in Fig. 3 that displays the time-resolved log-normal aggregate size distribution as a function of time after pH jump. The resolution of this property is unusual and is possible due to our ability to observe both the mean aggregate growth as well as the size distribution profile as a function of time with great detail. From these distribution plots, it is easy to reconcile the results from Fig. 2; the size distribution peaks shift to larger values with larger pH quench. However, it is the systematic behavior of the size distribution profiles that underscores our proposed mechanism on the pH dependence of nanoparticle aggregation.

For unexposed solutions, the peak and standard deviation remain unchanged, denoting a stable nanoparticle suspension [Fig. 2(a)]. In the case of shallow pH quenches (pH 5.06), the $R_{h,peak}$ does not shift, while σ_{R_h} shows a distinct increase, as seen in Figs. 2(b) and 3(a). This is clearly evidence of a metastable aggregate formation and dissolution with no significant shift in the $R_{h,peak}$. For intermediate pH quenches (pH \approx 5.0), the inception of small cluster growth indicative of RLCA behavior is seen through the more rapid increase in σ_{R_h} even as $R_{h,peak}$ remains unchanged in the early time scale after exposure [Fig. 3(b)]. As time continues, $R_{h,peak}$ begins to increase due to increasing stability of larger clusters, resulting in the increasing size trend shown in Fig. 2(b). Finally, for the deepest pH quenches, both $R_{h,peak}$ and σ_{R_h} immediately and strongly increase for all times after exposure, an expected behavior for DLCA [Fig. 3(c)].

It is also striking that this broad kinetic behavior exists within such a small pH range. The notion that the onset of instability of solution of molecules or suspension of particles is attributed to the ionic strength or charge state of the particles is quite common. However, it is clear that this system exhibits marginal stability within the parameter range studied. This sensitivity of aggregation to pH should be taken into account for future research or design of nanoparticle systems, especially for bioapplications.

As mentioned previously, the ionic nature of water-soluble PAGs poses an obvious limitation on the concentration range available to investigate for any charged system. Switching to a nonionic PAG system does not properly address this issue due to the need to use a mixed organic/aqueous solution to get the PAG to dissolve that may exacerbate nanoparticle solubility issues. This work may inspire new, innovative PAG types that may broaden the applicability for charged model systems.

The main goal of our work was to controllably drive the solution into an unstable state. By quenching the pH, a shift of the equilibria of the particle surface carboxylic acid groups effectively decreased the electrostatic repulsion between particles and reduced stability. A reduced stability of charged particle systems, such as polyelectrolytes, is commonly observed by decreasing temperature or increasing the solution ionic strength. Similarly, we envision making systematic explorations of the effect of pH changes on the stability of these suspensions through a consideration of how the effective pairwise interactions depend on pH, temperature, and ionic strength. In this way, we hope to develop stability criteria that better quantify the factors that influence the rapid particle aggregation kinetics.

IV. CONCLUSIONS

We utilize pH jumps using dissolved PAGs in aqueous solutions that form superacids upon UV exposure in conjunction with DLS as a model system to study the kinetics of nanoparticle aggregation. The characteristic time of the pH jump can be adjusted by the UV exposure dose conditions. When the exposure duration is shorter than the characteristic aggregation time, this approach provides a noninvasive method to follow the collective behavior with optical meth-

ods. DLS was demonstrated to characterize the *early time* kinetics of aggregation by integrating a broadband UV light source to a custom DLS setup that allows for detailed observation of *pH*-induced nanoparticle aggregation with <5 s resolution. For shallow *pH* quenches, little to no aggregation is observed. As the solution *pH* is brought toward the pK_a of the stabilizing charge moiety, the aggregation kinetics become very sensitive to *pH*, aggregation kinetic behavior consistent with reaction-limited cluster aggregation. For *pH* jumps at or below the pK_a , particle aggregation is rapid and exhibited kinetics consistent with diffusion-limited cluster aggregation. We propose that the kinetics of instability formation is rooted in the increased hydrophobic and secondary interaction forces as the surface charges are neutralized. We believe that further investigation of aggregation systems through a combination of enhanced experimental approaches and computer simulation would be insightful into the effectiveness of PAGs for use in complex fluid environments.

It has been shown^{23,24} that certain tumor cells exhibit a reduced, or even reversed, *pH* gradient across the cell membrane when compared to normal tissue. The *pH* gradients for each of the tumor cell types studied all fall within less than one *pH* unit, accessible within the *pH* range studied in this work. Since nanoparticles are expected for biomarkers for cellular imaging and identification, the technique described here could be used to directly measure the stability of nanoparticles that have been designed specifically to identify cancerous cells. Further, it has been shown that chemical composition, surface charge structure, and size are a few of the mitigating factors that determine the cellular toxicity of a nanoparticle system.^{25,26}

ACKNOWLEDGMENTS

R.J.M. acknowledges support through the National Research Council–National Institute of Standards and Technology (NIST) Postdoctoral Fellowship Program. We thank Dr. Nadia Edwin (NIST) for the technical assistance in nanoparticle handling and use of DLS during the initial stages of this

work. This is an official contribution of the National Institute of Standards and Technology; not subject to copyright in the United States.

- ¹B. Alberts, D. Bray, J. Lewis, M. Raff, K. Roberts, and J. D. Watson, *Molecular Biology of the Cell* (Garland Science, New York, NY, 2002).
- ²T. Kim, C. H. Lee, S. W. Joo, and K. Lee, *J. Colloid Interface Sci.* **318**, 238 (2008).
- ³M. Y. Lin, H. M. Lindsay, D. A. Weitz, R. Klein, R. C. Ball, and P. Meakin, *J. Phys.: Condens. Matter* **2**, 3093 (1990).
- ⁴J. F. Zhou, R. Sedev, D. Beattie, and J. Ralston, *Langmuir* **24**, 4506 (2008).
- ⁵M. Y. Lin, H. M. Lindsay, D. A. Weitz, R. C. Ball, R. Klein, and P. Meakin, *Phys. Rev. A* **41**, 2005 (1990).
- ⁶Y. T. He, J. M. Wan, and T. Tokunaga, *J. Nanopart. Res.* **10**, 321 (2008).
- ⁷S. H. Behrens, D. I. Christl, R. Emmerzael, P. Schurtenberger, and M. Borkovec, *Langmuir* **16**, 2566 (2000).
- ⁸J. M. Fedeyko, D. G. Vlachos, and R. F. Lobo, *Langmuir* **21**, 5197 (2005).
- ⁹I. N. Seekkuarachchi and H. Kumazawa, *Ind. Eng. Chem. Res.* **47**, 2391 (2008).
- ¹⁰F. Gröhn, K. Klein, and S. Brand, *Chem.-Eur. J.* **14**, 6866 (2008).
- ¹¹I. Willerich and F. Grohn, *Chem.-Eur. J.* **14**, 9112 (2008).
- ¹²J. D. Lewis, R. T. C. Ju, A. I. Kim, and S. L. Nail, *J. Colloid Interface Sci.* **196**, 170 (1997).
- ¹³J. J. Storhoff, R. Elghanian, R. C. Mucic, C. A. Mirkin, and R. L. Letsinger, *J. Am. Chem. Soc.* **120**, 1959 (1998).
- ¹⁴J. J. Storhoff, A. A. Lazarides, R. C. Mucic, C. A. Mirkin, R. L. Letsinger, and G. C. Schatz, *J. Am. Chem. Soc.* **122**, 4640 (2000).
- ¹⁵H. Ito, *Adv. Polym. Sci.* **172**, 37 (2005).
- ¹⁶R. R. Dammel, G. Pawlowski, A. Romano, F. M. Houlihan, W. K. Kim, R. Sakamuri, and D. Abdallah, *Proc. SPIE* **5753**, 95 (2005).
- ¹⁷W. Hinsberg, G. Wallraff, C. Larson, B. Davis, V. Deline, S. Raoux, D. Miller, F. Houle, J. Hoffnagle, M. Sanchez, C. Rettner, L. Sundberg, D. Medeiros, R. Dammel, and W. Conley, *Proc. SPIE* **5376**, 21 (2004).
- ¹⁸R. D. Allen, P. J. Brock, L. Sundberg, C. E. Larson, G. M. Wallraff, W. D. Hinsberg, J. Meute, T. Shimokawa, T. Chiba, and M. Slezak, *J. Photopolym. Sci. Technol.* **18**, 615 (2005).
- ¹⁹G. M. Wallraff, C. Larson, L. Sundberg, G. Breyta, M. Sanchez, H. Truong, B. Davis, R. Allen, D. Gil, V. Prabhu, and S. Sambasivan, Proceedings of the Second International Symposium on Immersion Lithography, Bruges, Belgium, 12–15 September 2005.
- ²⁰P. Štěpánek, *J. Chem. Phys.* **99**, 6384 (1993).
- ²¹J. C. Thomas, *J. Colloid Interface Sci.* **117**, 187 (1987).
- ²²F. G. Bordwell, *Acc. Chem. Res.* **21**, 456 (1988).
- ²³L. E. Gerweck and K. Seetharaman, *Cancer Res.* **56**, 1194 (1996).
- ²⁴J. A. Thomas, R. N. Buchsbaum, A. Zimniak, and E. Racker, *Biochemistry* **18**, 2210 (1979).
- ²⁵D. Maysinger, *Org. Biomol. Chem.* **5**, 2335 (2007).
- ²⁶C. J. Murphy, A. M. Gole, J. W. Stone, P. N. Sisco, A. M. Alkilany, E. C. Goldsmith, and S. C. Baxter, *Acc. Chem. Res.* **41**, 1721 (2008).